Accepted Manuscript

Microseismic noise in the Saint Peter and Saint Paul Archipelago, equatorial Atlantic

Daniel É. de Queiroz, Aderson F. do Nascimento, Martin Schimmel

PII: S0895-9811(16)30334-0

DOI: 10.1016/j.jsames.2017.09.035

Reference: SAMES 1800

To appear in: *Journal of South American Earth Sciences*

Received Date: 21 December 2016

Revised Date: 12 September 2017

Accepted Date: 30 September 2017

Please cite this article as: de Queiroz, Daniel.É., do Nascimento, A.F., Schimmel, M., Microseismic noise in the Saint Peter and Saint Paul Archipelago, equatorial Atlantic, *Journal of South American Earth Sciences* (2017), doi: 10.1016/j.jsames.2017.09.035.

MICROSEISMIC NOISE IN THE SAINT PETER AND SAINT PAUL ARCHIPELAGO, EQUATORIAL ATLANTIC

Daniel É. de Queiroz(1), Aderson F. do Nascimento(1, 2), Martin Schimmel(3)

(1) Programa de Pós-graduação em Geodinâmica e Geofísica – UFRN, Natal, Brazil

(2) Departamento de Geofísica – UFRN, Natal, Brazil

(3) Instituto de Ciencias de la Tierra “Jaume Almera” – CSIC, Barcelona, Spain

Abstract

Microseismic noise, also known as ambient seismic noise, are continuous vibrations mostly composed of Rayleigh waves pervasively recorded in the mili Hertz to 1 Hz frequency range. Their precise source mechanisms are under investigations and related to atmospheric perturbations and ocean gravity waves. Our purpose is to show the behavior of the microseismic noise recorded in the Saint Peter and Saint Paul Archipelago (SPSPA) with respect to wind intensity and ocean waves height in this region, between the North and South Atlantic Ocean. We have recorded both primary microseisms (PM) 0.04 – 0.12 Hz and the secondary microseisms (SM) 0.12 – 0.4 Hz during almost four years (2012 to 2015) and we used frequency, temporal, spatial and statistical correlation analysis to do qualitative and quantitative analysis with respect to wind speed intensity and significant wave height for the same periods. The results indicate a good correlation between the PM and the SM noise in the region particularly during the winter in the Northern Hemisphere and a poor correlation during the summer. We have also shown that probably most of the PM are generated in the SPSPA itself. We note that the intensity of SM recorded in SPSPA appears to have a seasonal behavior with the summer and winter in the Northern Hemisphere, and seems to influence the correlation between the PM and the SM, suggesting that the sources of the PM and the SM are not related to the same atmospheric event and from different places. PM generation would occur near the SPSPA whilst the SM would have distant sources towards the North Atlantic.

Key words: microseismic noise, primary microseisms, secondary microseisms, Saint Peter and Saint Paul Archipelago, wind speed, significant wave height, Atlantic Ocean.

1.0 Introduction

Microseismic noise (or ambient seismic noise) is pervasive in broadband records from few mili Hertz to about 1 Hertz. The weakest and strongest globally observed ambient noise are the hum and the microseisms, respectively. The Earth's hum [e.g., Suda et al., 1998; Tanimoto et al., 1998; Roult and Crawford, 2000; Rhie and Romanowicz, 2004] comprise free oscillations of the Earth around 4–20 mHz and are generated through infra-gravity waves in the shallow ocean. Microseismic noise, however, is mostly Rayleigh waves and is stronger in the 0.04 to 1 Hz frequency band. In this work we analyze only the microseismic noise.

Microseismic noise is divided into primary microseisms (PM) and secondary microseisms (SM). The PM (also called “single frequency peak”) exhibit dominant frequencies of 0.04 – 0.1 Hz whilst SM (or “double frequency peak”) have frequencies about 0.1 – 1 Hz [Longuet-Higgins, 1950; Haubrich et al., 1963; Hasselmann, 1963; Holcomb, 1980; Webb, 1992; Bromirski and Duennebier, 2002; Tanimoto, 2007; Webb, 2008; Schimmel et al., 2011]. The PM have the same frequencies as the ocean gravity waves and are caused by the interaction of ocean waves with the (sloping) sea floor [Hasselmann, 1963]. The SM are stronger signals caused by pressure oscillations through the interference of waves with the same frequency but with opposite directions [Longuet-Higgins, 1950; Hasselmann, 1963; Tanimoto, 2007; Ardhuin et al., 2011; Stutzmann et al., 2012; Gualtieri et al., 2013].

The SM are the strongest noise and dominate the microseismic energy spectrum. The SM generation areas have been observed near the coast [e.g., Friedrich et al., 1998; Bromirski and Duennebier, 2002; Schulte-Pelkum et al., 2004; Rhie and Romanowicz, 2006; Gerstoft and Tanimoto, 2007; Yang and Ritzwoller, 2008] and far from the coast in the deep ocean [e.g., Cessaro 1994, Stehly et al., 2006; Koper and de Foy, 2008; Gerstoft et al., 2008; Kedar et al., 2008; Obrebski et al., 2012; Obrebski et al., 2013; Gualtieri et al.,2014, Beucler et al., 2015].

The quantitative modeling of the SM is now possible thanks to ocean wave modeling, hindcasts and theoretical development based on Longuet-Higgins (1950) and normal mode summations [surface waves: Kedar et al., 2008; Ardhuin et al.,2011; Stutzmann et al., 2012; Gualtieri et al.,2013; body waves: Gualtieri et al.,2014]. These modeling studies show that the strongest SM sources are in the deep ocean which is also in agreement with Longuet-Higgins (1950). The analysis of the relationship of ocean wave spectra from offshore and nearshore buoys with SM at ocean bottom or inland seismic stations suggest that most of the microseisms are excited in nearshore areas [Zopf et al., 1976; Bromirski and Duennebier, 2002]. Additionally, several microseismic noise studies have focused on identifying their sources by correlating their data with the significant ocean wave height (Hs) and period (Ts) [Tindle and Murphy, 1999; Bromirski et al., 1999; Traer et al., 2012], wind speed and storms [Bromirski, 2001; Bromirski and Duennebier, 2002; Bromirski et al., 2005; Gerstoft et al., 2006; Gerstoft et al., 2008; Aster et al., 2010], and seasonality [Gerstoft and Tanimoto, 2007; Stutzmann et al., 2009; Schimmel et al., 2011; Grob et al., 2011; Reading et al., 2014].

Here, we present the analysis of microseismic noise from a broadband station in the Saint Peter and Saint Paul Archipelago (SPSPA) (see location in Fig. 1) and show the behavior of the microseismic noise with respect to wind speeds and ocean waves height in this region, between the North and South Atlantic Oceans. We focus on observing the seasonal behavior, especially of SM, with respect to the summer and the Northern Hemisphere winter. We use seismological, wind speed, significant wave height and peak wave period data for the period between 2012 and 2015.

The SPSPA is located in the equatorial region of the Atlantic Ocean (00º55.1' N, 29º20.7' W) about 1,100 km distant from the Brazilian northeastern coast and is composed by a set of several small rocky formations (see Fig. 1) that rises from approximately 4,000 m from the sea floor as shown in Fig. 2.

2.0 Study area

The SPSPA has a total area of approximately 17,000 m², a maximum altitude above the mean sea level of 18 m.The greatest distance between the furthermost points is around 420 m [Miguens, 1995]. The environmental conditions for human life in the SPSPA are quite severe due to the seismic and meteorological activities, and the lack of vegetation and potable water. In addition, seismicity in the vicinity of the SPSPA and along the Saint Paul Transform Fault Zone is mainly characterized by strike-slip earthquakes [Angulo et al., 2013]. However, earthquakes with body-wave magnitude equal or greater than 5.4 related to reverse faulting have also been reported in the last decades [Wolfe et al., 1993]. Fig. 2A shows the bathymetry in the SPSPA and the main fault kinematics.

Geologically speaking, the SPSPA is an outcrop of the sub-ocean mantle and is a rare case of islet formation from a tectonic fault [Motoki et al., 2009, 2010]. The SPSPA is the emerged part of a submarine mountain chain which has approximately 400 km². SPSPA bathymetry (see Fig. 2) shows that this mountain chain has an underwater landscape with crest-like elevations with a gentle slopes towards the EW direction and a steep slope in the NS direction. This NS direction slope lies parallel to the north side of the Saint Paul Transform fault zone, quite close to the South-American and African Plates divergence [Mabesoone and Coutinho, 1970; Bonatti, 1990; Hekinian et al., 2000; Campos et al., 2010].

Despite the harsh conditions, the SPSPA is permanently occupied by the Brazilian Navy with military and/or research staff in the existing scientific base. Since 2012 a broadband seismic station has been operating in the SPSPA.

The SPSPA is close to the equator which makes this station unique since it allows to relate northern and Southern Hemisphere climate perturbations through seismic noise observed in the middle of the Atlantic Ocean. Due to the distance from the continent and the lack of cultural noise, the SPSPA is a unique location for measuring microseismic noise and investigating its relationship with wind speeds and ocean waves.

This is the first study carried out which characterizes the noise at station SPSPA, permitting future climate monitoring studies, unbiased from anthropogenic activities.

3.0 Data

3.1 Data from broadband seismic station

We used instrument corrected broadband seismic records between 2012 and 2015 record from a seismic station in the SPSPA. The vertical component data were originally sampled at 100 Hz and then decimated to 2 Hz for spectral analysis.

3.1.1 Power Spectral Density (PSD)

For the power spectral density (PSD) estimation, we use the method by Welch (1967). This method is standard in signal processing (e.g. Brillinger, 2001; Bendat and Piersol, 2012) and is based on the use of the classical periodogram spectrum estimation but reducing the noise due to imperfect and finite length data in the estimated power spectra. Fig. 3 shows the result of the PSD for August 2012. We can identify the PM and the SM with frequency bands of 0.04 – 0.12 Hz and 0.12 – 0.4 Hz. Additionally, the Gulf of Guinea microseism [Shapiro et al.,2006, Yingjie Xia et al., 2013] is visible at at frequencies of about 0.038 Hz. The hum is not seen in this figure.

3.1.2 Spectrogram

To illustrate the time frequency content of the broadband recorded seismic data, we computed the spectrogram using the short-time Fourier transform method from year 2012 until 2015 shown in Fig. 4a-d. The gaps in dark blue correspond to periods without recorded data. To compute the time-frequency representation of the data, we used the vertical component data sampled at 2 Hz. Plotted are the daily averages of the spectra obtained from

1024 sample long sliding data windows and 50% window overlap. We can identify that the spectrogram for frequencies below 0.5 Hz exhibit two frequency bands where most energy is concentrated. The first one is 0.04 – 0.12 Hz (PM) and the second band is 0.12 – 0.4 Hz (SM). For all years analyzed the spectrogram shows seasonal variations, i.e., approximately from June to September the SM frequency band is narrower due to decreased amplitudes than during other periods of the year (September to February). This seasonal variation is not observed for the PM.

3.1.3 PM and SM spectral amplitude

We also computed the mean amplitude spectra of the broadband data. Firstly we separated the PM and the SM by band pass two-pole filters using the cutoff frequencies shown in Fig. 3 (PM = 0.04 – 0.12 Hz and SM = 0.12 – 0.4 Hz). The result of this procedure is to obtain two time series: one containing PM data and a second one containing SM data. Secondly, we take the absolute value of each of the (PM or SM) time series, then we resample the data to 1 sample/hour, remove the spikes and normalized the data by dividing each amplitude value of the time series by its norm-2 value.

Fig. 5 shows the result of the above described procedure. The amplitude of the PM (black line) and the SM (red line) computed for the years 2012 (a), 2013 (b), 2014 (c) and 2015 (d). The periods without data are the same as those shown in Fig. 4. The light grey area between June and September suggests, qualitatively, that the PM and SM mean amplitudes are not similar. Both, PM and SM seem to have a different trend. It can be seen that during Jun-Aug increased amplitude PM events are not accompanied by increased SM amplitude events, which is different for what can be seen for the rest of the months. The months marked in grey correspond to the same time of the year when a decrease of the SM frequency range is visible in Fig. 4. This is particularly observed in Fig. 5 (a) and (b) corresponding to 2012 and 2013, respectively. On the other hand, it is observed that the PM and SM mean amplitudes are nearly similar outside this period. This is especially observed in 2012 (a) about mid of September until December, in 2013 (b) from April until half of May and from September until December in 2014. Generally speaking, we observe that the SM amplitudes decreases more (Jun-Aug) than PM amplitudes – specially for 2012, 2013 and 2015. Figure 5 shows that PM has no amplitude maximum which is not accompanied by an increase the rest of the year, whilst during June, July and August PM maxima seem not to be correlated or overwhelmed by SM.

3.2 Ocean wave and wind speed data

We investigate the relationship between broadband data and environmental data such as ocean wave significant height (Hs) and wind speed (Ws). We used hourly averaged Hs, Tp and Ws data from the model WaveWatch III (WW3) [Tolman, 2009] available from the National Center for Environmental Prediction (NCEP) at http://polar.ncep.noaa.gov/. We have data available from six locations as shown in Fig. 1. Locations 44141, 62002 (Northern hemisphere), 'Rio Grande' and 'Agulhas FA' (Southern hemisphere) are used for computing daily average of Hs along from years 2012 until 2015. Locations 41041, 'Amazon' and 'SPSPA' are those we use to analyze the relationship between microseismic noise and Hs. For wind intensity maps we show, we used the data from the National Oceanic and Atmospheric Administration/National Climatic Data Center (NOAA/NCDC) that provides the multi-satellite product Blended Sea Winds (BSW) which we used to obtain wind speed. The BSW product combines several (both passive and active) remote sensing observations via Gaussian interpolation to increase both temporal and spatial resolution [Zhang et al., 2006]. Therefore, the wind data we had available has a spatial resolution of 0.25deg and a temporal resolution of 6 hours. We use the same methodology used in Silva et al., 2016 to generate wind speed maps.

3.2.1 Wave significant height

We present in Fig. 6a the annual variation of Hs for locations 44141, 62002 (Northern hemisphere), from 2012 until 2015. We present in Fig. 6b a similar plot for the locations 'Rio Grande' and 'Agulhas FA' (Southern hemisphere) for the same period. In Figs. 06c-e we present the annual variation of Hs, peak wave period (Tp) and wind intensity for locations SPSPA for the 2012-2015 period. The thick black line in each of these plots is the 10th order polynomial fitting of the average of each data point for the four years available. The ideal to use such a high order polynomial is to smooth the data and exhibit only a tendency of the data. We can observe for the daily average along of Hs in North Atlantic (Fig. 6a) the months between June and September are the ones that show the lowest Hs average, i.e., the period with less intense wave heights. As for the South Atlantic (b), the months between June and September show the highest average Hs. In Fig. 6d and 6d, we do not observe any major variations in average Hs and Tp, respectively, in the SPSPA location. The wind velocity shown in Fig. 6e has a gradual increase beginning approximately mid May, reaching a plateau in July and maintaining higher values until December.

3.2.2 Wind intensity maps

We now present in Fig. 7 the wind intensity maps (in m/s) for the years analyzed (2012-2015). We present only January—March (left column of Fig. 7, i.e., Figs. 7a, c, e, g) and July—September (right column of Fig. 7, i.e., Figs. 7a, c, e, g) periods as they are representative of the winter and summer in the northern hemisphere, respectively. Warm colors for greater wind intensity as opposite to cold ones. We see clearly that for all years (2012 to 2015), the months between January and March the strongest winds are in the North Atlantic (see left column—a, c, e, g). On the other hand, for the months between July and September the strongest winds are in the South Atlantic (see column right—b, d, f, h).

4.0 Results

4.1 Correlation coefficients between PM and SM

To quantify the correlation between PM and SM, we use the Pearson Pearson correlation value (*r*) (Press et al., 1992) for the years 2012–2015 in

Figure 8. High (close to one) positive values indicate that the relationship between the variables (the PM and the SM) has the same trend. Negative values indicate the opposite trend. Values close to zero indicate no relationship between the variables. We computed *r* only for the months that had more than 50% of continuous data, and correlation confidence level equal to or more than 95%. Except for 2014, in which September had the highest *r* value for this year, we can see clearly that the lowest correlation (including an anti-correlation in June 2013) in each year are usually between June and September, indicating poor association between the PM and the SM in these periods. In 2014, instead, the period with the lowest value of *r* is for the June—August period. This period (June—September) is the same when apparently the PM and the SM mean amplitudes are not similar seen in (Fig. 5 light grey area) and a decrease of the SM is seen in Fig. 4. For the remaining months, when the SM increases (Fig. 4, we see in general, higher values of correlations indicating good association between the PM and the SM in these periods of time. This three-month period coincides with the one exhibiting an overall decrease in the correlations values between the PM and the SM in each year shown in Fig. 8. However, it is important to stress that an amplitude decrease could mean a decrease of sea activity while the decrease of correlation between PM and SM indicates that the PM and SM sources are not caused by the same meteorological perturbation at the sea.

4.2 Amplitudes PM, SM and Hs

We now integrate the information from PM, SM and Hs to investigate the influence and possible origin of the microseismic noise in the SPSP. For this analysis as mentioned previously, we use Hs data from locations SPSP, 41041 and 'Amazon'. For the sake of clarity, we only show PM, SM and Hs data for a few months and some locations. We have produced figures for entire four-year period as supplemental material as Figures S1-S12. Figs. 9, 10 and 11 compares the amplitudes of the PM, SM and Hs (locations SPSP, 41041 and 'Amazon') for the months of July, October and December 2012, respectively. These months are shown because they are representative of our results. We use normalized data and sampling rate of one sample per hour. In Fig. 9a we clearly see a low correlation between PM and SM in July 2012 (see July in figure 8a, r = 0.039). Fig. 9b shows that location SPSP exhibit two maxima for Hs which coincide with the two PM maxima (days from 6th until 12th July 2012 and 18th until 22nd July 2012 in hi-lighted in grey). Now, Fig. 9c we observe now that the maximum in SM amplitude coincides with a maximum of Hs in location 41041 (days from 12th until 17th July 2012). Fig. 10a clearly shows a high correlation between PM and SM in October 2012 (see October in Fig. 8a, r = 0.6). Fig. 10b compares now PM, SM and Hs in location 'Amazon'. We here, observe a coincidence in the highest values of PM with Hs from days 9th until 16th October 2012. In Fig. 10c we also observe a coincidence of maxima between SM and Hs for location SPSP for the same period. Fig. 11a clearly shows a high correlation between amplitudes of the PM and the SM of December 2012 (see December in Fig. 8a, r = 0.7). In Fig. 11b we note that the values of PM coincide with those from location SPSP between 10th and 28th December 2012. Fig. 11c compares the PM, SM and Hs for location 41041 but for this case, we do not observe similarity between these data from 10th and 28th December 2012 (as we have observed in Fig. 9b for location 41041, for instance).

Discussion of Results

According to Stutzmann et al., (2009) the strongest sources of microseisms in the Atlantic Ocean are between January and February in the North Atlantic and between July and August in the South Atlantic. According to Bromirski et al., (2005) the lack of correlation between the PM and the SM is an indicator that those signals are generated at different locations, for example at different places due to different phenomena.

Here, we have shown that the relationship between the PM and the SM is seasonal and the best correlation between them is during the Northern Hemisphere winter (Fig. 8). During the Southern Hemisphere winter the correlation is very low and therefore the PM and the SM probably have different sources. This seasonality is seen by observing the narrowing of the SM frequency band in Fig. 4 in the period close to the summer in the Northern Hemisphere (about June to September), when the wind intensity decreases in the North Atlantic (see Figs. 8b, d, f and h). On the other hand, the period close to the winter in the Northern Hemisphere (around January until March) exhibits increased SM energy as shown in Fig. 4, and appears to be associated with increased wind intensity in the North Atlantic (see Figs. 8a, c, e and g). We reckon that wind direction is an important data that could be used as it provides the direction of the swell that may generate PM at the coast and SM through interference with other swell (reflected from a coast or another storm) at similar frequency and opposite direction. However, this data was not available and this association could not be observed.

This seasonality is displayed quantitatively in the correlation of Fig. 8. This seasonality in SM recorded in SPSPA indicates the possibility of having sources of the PM and the SM in different locations, especially for the months of lowest correlation between the PM and the SM (about June until September- see Fig. 8). This possibility is seen in the analysis of Figs 9, 10 and 11. In Fig. 9, when there is low correlation between the PM and the SM (Fig. 9a) the PM appear to have good relationship with the local Hs (recorded at SPSPA and shown in Fig. 9b), and the SM appear to be well associated with Hs far from SPSPA recorded near the location 41041 (Fig. 9c). In Fig. 10, where there is a high correlation between the PM and the SM (Fig. 10a), we see that both the PM and the SM seem to have a good relation with Hs away from the SPSPA near the 'Amazon' location (Fig. 10b), and a smaller connection with the local Hs at SPSPA (Fig. 10c). In Fig. 11, there is also a high correlation between the PM and the SM (Fig. 11a), and we see that both the PM and the SM seem to have a good relationship to Hs in the SPSPA itself, but a smaller association to Hs near location 41041 (Fig. 11c), the same that was shown to have a good association with SM in Fig. 9c.

Although the SPSPA is located in the equatorial region and its climate variables (Fig. 6c-e) show no relationship with Hs and wind intensity in the Northern Hemisphere, the correlation between the PM and the SM is appears to be controlled by the Northern Hemisphere seasonality. Probably, SM recorded in the SPSPA are dominated by the Northern Hemisphere seasonality. During the summer in that region, SM are generated in most cases away from the SPSPA; during the Northern Hemisphere winter, SM generation is related to the same swell that arrives the island to generate the PM at its coastline and which therefore explains the increased correlation between both. Swell can travel over large distances for a week or more which would permit to have PM and SM sources generation far from each other, but this would also imply a systematic time shift between PM and SM (Fig. 5), which is not observed for Northern Hemisphere winter. Based on that and the comparison to Hs measurements we conclude that the SM noise probably is generated close to the SPSPA itself. If this interpretation is correct then swell reflection is likely a reason to generate the opposed swell as required for SM generation (Ardhuin et al. 2011).

5.0 Conclusions

This study showed seasonality between microseismic noise, wind speed and wave height in a particular region located in the center of the Atlantic Ocean close to the Equator. The SPSPA noise recordings indicate that the microseismic noise on the island is dominated by Northern Hemisphere climate. It has been shown that PM and SM noise activity is correlated during Northern Hemisphere winter, and most of the year with exception of the Southern Hemisphere winter. No significant time shifts are observed for the correlations. Also based on our comparisons with Hs measurements this correlation is interpreted by an SM generation not too far from the Island where the PM noise is generated at the coast. The opposed swell for SM generation could be due to Island reflections. During Southern Hemisphere winter, PM and SM are not related which we interpret as due to different climatic phenomena. The SM is likely generated far from the Island. Further studies are required to verify these hypotheses. The gaps in the records of seismological data somewhat limited our quantitative and qualitative interpretations about seasonality. In addition, as our goal was not specifically to locate sources of the PM and the SM, it is important to emphasize that this has limited our interpretations about the origin of the PM and the SM recorded in the SPSPA.

The seismic station at SPSPA is probably the only seismic station near the Mid Atlantic ridge in the equatorial area. This station is therefore unique for very different types of seismological studies. Here, we started with a characterization of the microseismic noise from continuous records of almost four years.

Acknowledgment

The authors thank the support of the Navy of Brazil. Allan Silva and Mario Silva also are thanked for their for their help with the ocean and wind data. The authors acknowledge the Editor, Marcelo Assumpção and two anonymous reviewers for handling and improving the manuscript with their constructive comments. AFdN and MS thank CNPq for the grant 402174/2012-7 (Science without Borders Programme), AFdN thank CNPq for grants 484441/2012-4 and 303817/2014-3.

FIGURE CAPTIONS

Fig. 1: Location map of the SPSPA with location of the buoys used in this study, and an aerial photo of the area. The extreme points of the SPSPA have approximately 450 m (source of the aerial photo: http://www.popa.com.br/_2008/imagens/paisagens/paisagens_778.htm).

Fig. 2: (a) map showing the bathymetry of the area and the Saint Paul Transform Fault Zone. The triangle denotes the location of the Saint Peter and Saint Paul Archipelago (SPSPA). The lines denote the strike-slip and thrust fault kinematics in the area. (b) 3D visualization of the bathymetry around the SPSPA (modified from Sichel *et al.*, 2008) showing the mountain chain with gentle slope towards the EW direction and a strong slope in the NS directions. The water depths around the SPSPA is around 4,000 m and the area shown has approximately 400 km². The vertical scale is exaggerated 12 times relative to horizontal scale.

Fig. 3: Welch Power Spectra Density (PSD) for August 2012 in the SPSPA showing the Primary Microseisms (PM) with frequency 0.04 – 0.12 Hz and Secondary Microseisms (SM) with frequency 0.12 – 0.4 Hz.

Fig. 4: Spectrogram of microseismic energy distribution for the SPSPA station for 2012 (a), 2013 (b), 2014 (c) and 2015 (d). We highlight the PM bandwidth (0.04 – 0.12 Hz) and the SM bandwidth (0.12 – 0.4 Hz).

Fig. 5: Amplitude of the microseisms recorded at SPSP for 2012 (a), 2013 (b), 2014 (c) and 2015 (d). PM (0.04 - 0.12 Hz) in red and SM (0.12 - 0.4 Hz) in black. The grey stripe highlights the period in which PM and SM are poorly correlated.

Fig. 6: Interpolation (thick black line) of the daily average along the year of significant wave height (Hs) for two location (44141 and 62002) in the Northern Atlantic (a) and two buoys (RIO GRANDE and AGULHAS FA) for the Southern Atlantic (b). It also shows the daily average interpolation (thick black line) of these four years (2012 to 2015) to Hs (c), peak wave period (d) and wind speed (e) in the location SPSPA.

Fig. 7: Wind Intensity map (in m/s) of ocean wind along the Atlantic Ocean (warmer colors for greater wind intensity). The left column (a, c, e, g) are for the months of January to March (Winter in the Southern Hemisphere - showing a greater wind intensity in the Southern Hemisphere) and the right column (b, d, f, h) are for the months of July to September (winter in the Northern Hemisphere - showing a greater wind intensity in the Northern Hemisphere) for the years 2012 (a, b), 2013 (c, d) 2014 (e, f) and 2015 (g, h).

Fig. 8: Pearson monthly correlation values (r) between PM and SM amplitudes for 2012 (a), 2013 (b), 2014 (c) and 2015 (d). High (close to one) positive values indicate that the relationship between the variables (the PM and the SM) has the same trend. Negative values indicate the opposite trend. Values close to zero indicate no relationship between the variables. r is computed for the months having more than 50% of continuous data, and correlation confidence level equal to or greater than 95%.

Fig. 9: Normalized amplitude values for July 2012. (a) Normalized amplitude for the PM and the SM showing a poor correlation between those two variables; (b) Normalized amplitude for the PM and the Hs in SPSP showing that the maxima between these two variables coincides for nearly the entire month (we highlight the period in which this coincidence appears); (c) Normalized amplitude for SM and Hs in location 41041 (we highlight the period in which the maxima coincide).

Fig. 10: Normalized amplitude values for October 2012. (a) Normalized amplitude for PM x SM showing a good correlation between those two variables. (b) Normalized amplitude for PM x Hs in Amazon showing that the maxima between these two variables coincides (we highlight the period in which this coincidence appears); (c) Normalized amplitude for the PM, SM and Hs at SPSPA (we highlight the period shown in (b).

Fig. 11: Normalized amplitude values for December 2012. (a) Normalized amplitude for the PM and the SM showing a good correlation between those two variables hence indicating the same source for the PM and the SM; (b) Normalized amplitudes for the PM, the SM and the Hs at SPSP showing showing that the maxima between these two variables coincides (we highlight the period in which this coincidence appears); (c) Normalized amplitudes for the PM, the SM and the Hs at location 41041 (we highlight the period shown in (b)).

Fig. S1-12: Supplemental figures showing PM, SM and Hs data

REFERENCES

Angulo, R. J., de Souza, M. C., Campos, T. F., Bezerra, F. H., Fernandes, L. A., Giannini, P. C. F., ... & Veiga, F. A. (2013). Evidence for Late Quaternary episodic uplift of the São Pedro and São Paulo Archipelago, Equatorial Atlantic. *Quaternary international*, *317*, 102-111.

Ardhuin, F., E. Stutzmann, M. Schimmel, and A. Mangeney (2011), Ocean wave sources of seismic noise, J. Geophys. Res., 116, C09004, doi:10.1029/2011JC006952.

Aster, R. C., McNamara, D. E., Bromirski, P. D., (2010), Global trends in extremal microseism intensity, Geophys. Res. Lett., Vol. 37, L14303, doi:10.1029/2010GL043472

Bendat, J. S., & Piersol, A. G. (2011). Random data: analysis and measurement procedures (Vol. 729). John Wiley & Sons.

Beucler E., Mocquet A., Schimmel M., Chevrot S., Quillard O., Vergne J., Sylvander M., Observation of deep water microseisms in the North Atlantic Ocean using tide modulations, Geophys. Res. Lett., 42, doi: 10.1002/2014GL062347, 2015.

Bonatti, E. (1990), Subcontinental mantle exposed in the Atlantic Ocean on St Peter-Paul islets. Nature, v. 345, p.800-802, 1990.

Brillinger, D. R. (2001). Time series: data analysis and theory. Society for Industrial and Applied Mathematics.

Bromirski, P. D., R. E. Flick, and N. Graham (1999), Ocean wave height determined from inland seismometer data: Implications for investigating wave climate changes in the NE Pacific, J. Geophys. Res., 104(C9), 20753–20766, doi:10.1029/1999JC900156.

Bromirski, P. D. (2001), Vibrations from the ‘‘perfect storm’’, Geochem. Geophys. Geosyst., 2(7), doi:10.1029/2000GC000119.

Bromirski, P. D., and F. K. Duennebier, (2002). The near-coastal microseism spectrum: Spatial and temporal wave climate relationships Journal of Geophysical Research, Vol. 107, No. B8. (22 August 2002), 2166, doi:10.1029/2001jb000265

Bromirski, P. D., F. K. Duennebier, and R. A. Stephen (2005), Mid-ocean microseisms, Geochem. Geophys. Geosyst.,6, Q04009, doi:10.1029/2004GC000768.

Campos et al.,(2010), Holocene tectonic uplift of the St Peter and St Paul Rocks (Equatorial Atlantic) consistent with emplacement by extrusion. Marine Geology (Print), p. 177-186, 2010.

Cessaro, R. K. (1994), Sources of primary and secondary microseisms, Bull. Seismol. Soc. Am., 84, 142–148.

Friedrich, A., F. Kruger, and K. Klinge (1998), Ocean-generated microseismic noise located with the Grafenberg array, J. Seismol., 2, 47– 64.

Gerstoft, P., M. C. Fehler, and K. G. Sabra (2006), When Katrina hit California, Geophys. Res. Lett., 33, L17308, doi:10.1029/2006GL027270.

Gerstoft, P., and T. Tanimoto (2007), A year of microseisms in southern California, Geophys. Res. Lett., 34, L20304, doi:10.1029/2007GL031091.

Gerstoft, P., P. M. Shearer, N. Harmon, and J. Zhang (2008), Global P, PP, and PKP wave microseisms observed from distant storms, Geophys. Res. Lett., 35, L23306, doi:10.1029/2008GL036111.

Grob, M., Maggi, A., Stutzmann, E., (2011), Observations of the seasonality of the Antarctic microseismic signal, and its association to sea ice variability, Geophys. Res. Lett., Vol. 38, L11302, doi:10.1029/2011GL047525

Gualtieri L., Stutzmann E., Farra V., Capdeville Y., Schimmel M., Ardhuin F., Morelli A. (2014), Modelling the ocean site effect on seismic noise body waves, Geophys. J. Int., doi: 10.1093/gji/ggu042, 2014.

Gualtieri L., Stutzmann E., Capdeville Y., Ardhuin F., Schimmel M., Mangeney A., Morelli A. (2013), Modelling secondary microseismic noise by normal mode summation, Geophys. J. Int., doi:10.1093/gji/ggt090, 2013.

Hasselmann, K., (1963). Statistical analysis of the generation of microseisms. Rev. Geophys. 1: 177–210.

Haubrich, R. A.,W. H.Munk & F. E. Snodgrass, (1963). Comparative spectra of microseisms and swell. Bull. Seism. Soc. Am. 53: 27–37.

Hekinian, R. et al.,(2000), Submersible observations of Equatorial Atlantic Mantle: The St. Paul Fracture Zone region. Marine Geophysical Research, v. 21, p. 529-560, 2000.

Holcomb, L. Gary. (1980), Microseisms: A twenty-six-second spectral line in long-period earth motion Bulletin of the Seismological Society of America, August 1980, v. 70, p. 1055-1070

Kedar, S., M. Longuet-Higgens, F. Webb, N. Graham, R. Clayton, and C. Jones (2008), The origin of deep ocean microseisms in the North Atlantic Ocean, Proc. R. Soc., Ser. A, 464, 777–793, doi:10.1098/rspa.2007.0277.

Koper, K. D., and B. de Foy (2008), Seasonal anisotropy of short-period seismic noise recorded in South Asia, Bull. Seismol. Soc. Am., vol. 98, No. 6), doi:10.1785/0120080082.

Longuet Higgins, M. S., (1950). A Theory on the origin of microseisms. Philos. Trans. R. Soc. Lond. A. 243: 1–35.

Mabessoone, J. M.; Coutinho, P. N. (1970), Litoral and shallow marine geology of northern and northeastern Brazil. Trabalhos. Oceanogr. Univ. Fed. de PE., Recife, v. 12, p. 1-214, 1970.

Miguens, Altineu P. (1995), Coastal Shipping, Estimated and Restricted Waters. Volume I. Directorate of Hydrography and Navigation of the Navy. Rio de Janeiro, 1995.

Obrebski, MJ., Ardhuin, F., Stutzmann, E., Schimmel, M., (2012), How moderate sea states can generate loud seismic noise in the deep ocean, Geophys. Res. Let., 39, 11, doi:10.1029/2012GL051896.

Obrebski, MJ., Ardhuin, F., Stutzmann, E., Schimmel, M., (2013), Detection of microseismic compressional (P) body waves aided by numerical modeling of oceanic noise sources, J. Geophys. Res.: Solid Earth 118 (8), 4312-4324, doi:10.1002/jgrb.50233.

Press, W. H., Teukolsky, S. A., Vetterling, W. T., & Flannery, B. P. (1992). Numerical recipes in fortran 77. 1992. Cambridge University, New York.

Reading, AM and Koper, KD* and Gal, M and Graham, LS and Tkalcic, H* and Hemer, MA*, “Dominant seismic noise sources in the Southern Ocean and West Pacific, 2000–2012, recorded at the Warramunga Seismic Array, Australia”, Geophysical Research Letters, 41 (10) pp. 3455-3463. doi:10.1002/2014GL060073

Rhie, J., and B. Romanowicz (2004), Excitation of Earth’s continuous free oscillations by atmosphere-ocean-seafloor coupling, Nature, 431, 552–556.

Rhie, J., and B. Romanowicz (2006), A study of the relation between ocean storms and the Earth's hum, Geochem. Geophys. Geosyst., 7, Q10004, doi:10.1029/2006GC001274.

Roult, G. and W. Crawford (2000). Analysis of 'background' free oscillations and how to improve resolution by subtracting the atmospheric pressure signal. Phys. Earth Plan. Int. 121: 325-338.

Schimmel, M., E. Stutzmann, F. Ardhuin, and J. Gallart (2011), Polarized Earth's ambient microseismic noise, Geochem. Geophys. Geosyst., 12, Q07014, doi:10.1029/2011GC003661.

Schulte-Pelkum, V., P. S. Earle, and F. L. Vernon (2004), Strong directivity of ocean-generated seismic noise, Geochem. Geophys. Geosyst., 5, Q03004, doi:10.1029/2003GC000520.

Shapiro, N.M., Ritzwoller, M.H., Bensen, G.D., (2006), Source location of the 26 sec microseism from cross-correlations of ambient seismic noise, Geophys. Res. Let., 33, 18, DOI: 10.1029/2006GL027010

Silva, A. R., Pimenta, F. M., Assireu, A. T., & Spyrides, M. H. C. (2016). Complementarity of Brazil′ s hydro and offshore wind power. *Renewable and Sustainable Energy Reviews*, *56*, 413-427.

Stehly, L., M. Campillo, and N. M. Shapiro (2006), A study of the seismic noise from its long-range correlation properties, J. Geophys. Res., 111, B10306, doi:10.1029/2005JB004237.

Stutzmann, E., Schimmel, M., Patau, G., Maggi, A., (2009), Global climate imprint on seismic noise, Geochem. Geophys. Geosyst., Vol. 10, No. 11, Q11004, doi:10.1029/2009GC002619

Stutzmann, E., Ardhuin, F., Schimmel, M., Mangeney, A., Patau, G. (2012), Modelling long-term seismic noise in various environments , Geophys. J. Int. , doi: 10.1111/j.1365-246X.2012.05638.x, 2012.

Suda, N., Nawa, K. & Fukao, Y., (1998), Earth's background free oscillations, Science, 279, 2089–2091.

Tanimoto, T., Um, J., Nishida, K. & Kobayashi, N., (1998), Earth's continuous oscillations observed seismically quiet days, Geophys. Res. Lett., 25, 1553–1556.

Tanimoto, T. (2007), Excitation of microseisms, Geophys. Res. Lett., 34, L05308, doi:10.1029/2006GL029046.

Tolman, H. L., (2009): User manual and system documentation of WAVEWATCH III version 3.14. NOAA / NWS / NCEP / MMAB Technical Note 276, 194 pp.+ Appendices

Traer, J., P. Gerstoft, P. D. Bromirski, and P. M. Shearer (2012), Microseisms and hum from ocean surface gravity waves, J. Geophys. Res., 117, B11307, doi:10.1029/2012JB009550.

Webb, S. C., (1992), The equilibrium oceanic microseism spectrum, J. Acoust. Soc. Am., Vol. 92,No. 4-1, pp. 2141-2158, doi:10.1121/1.405226

Webb, S. C., (2008), The Earth's hum: the excitation of Earth normal modes by ocean waves, Geophys. J. Int., Vol. 174, pp. 542-566, doi:10.1111/j.1365-246X.2008.03801.x

Welch, P.D, (1967), "The Use of Fast Fourier Transform for the Estimation of Power Spectra: A Method Based on Time Averaging Over Short, Modified Periodograms," IEEE Trans. Audio Electroacoustics, Vol. AU-15 (June 1967), pp.70-73.

Wolfe, C.J., Bergman, E.A., Solomon, S.C., (1993), Oceanic transform earthquakes with unusual mechanism or locations: relation to fault geometry and state of stress in the adjacent lithosphere. Journal of Geophysical Research 98, 16187e16211.

Xia, Y., Ni, S., & Zeng, X. (2013). Twin enigmatic microseismic sources in the Gulf of Guinea observed on intercontinental seismic stations. *Geophysical Journal International*, *194*(1), 362-366.

Yang, Y., and M. H. Ritzwoller (2008), Characteristics of ambient seismic noise as a source for surface wave tomography, Geochem. Geophys. Geosyst., 9, Q02008, doi:10.1029/2007GC001814.

Zhang, H.-M.; Reynolds, R. W.; Bates, J. J. (2006), Blended and gridded high resolution global sea surface wind speed and climatology from multiple satellites: 1987–present. In: American Meteorological Society 2006 Annual Meeting, Paper P. [S.l.: s.n.], 2006. v. 2.

Zopf, D. O., H. C. Creech, and W. H. Quinn (1976), The wavemeter: A land-based system for measuring nearshore ocean waves, Mar. Technol. Soc. J., 10, 19–25.

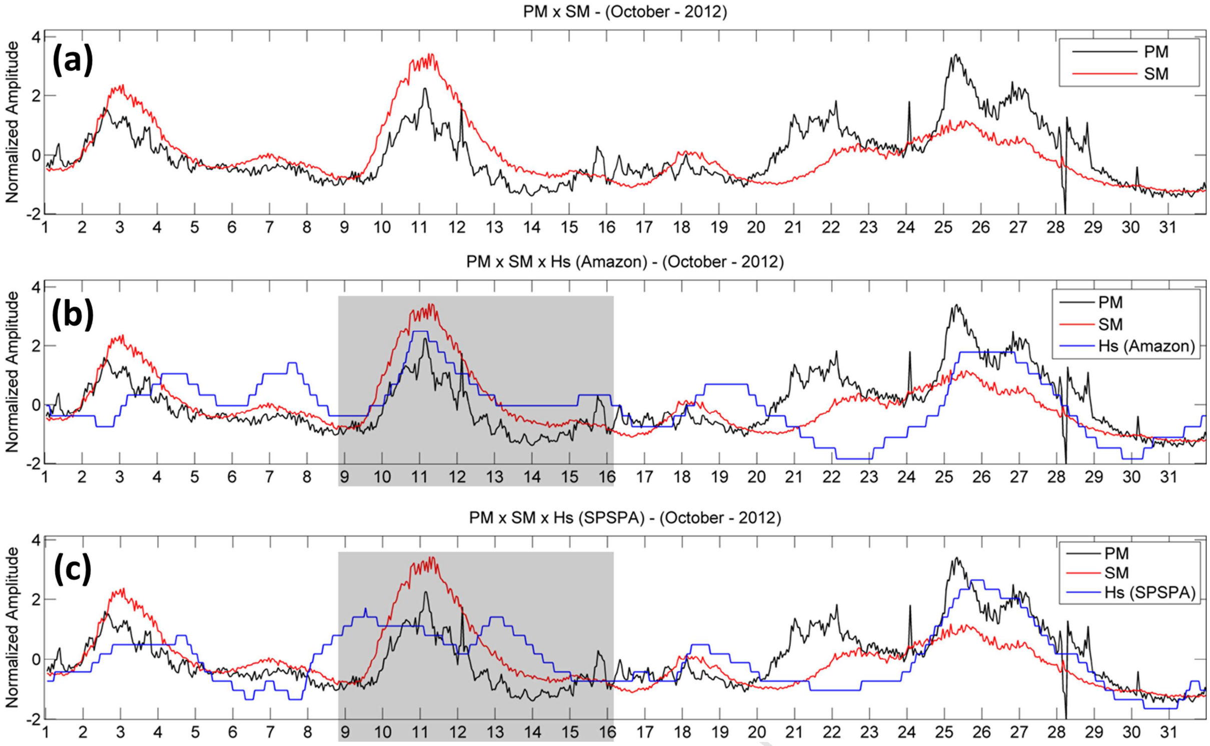
PM x SM - (October - 2012)
(a)
Normalized Amplitude
PM
SM
PM x SM x Hs (Amazon) - (October - 2012)
(b)
Normalized Amplitude
PM
SM
Hs (Amazon)
PM x SM x Hs (SPSPA) - (October - 2012)
(c)
Normalized Amplitude
PM
SM
Hs (SPSPA)

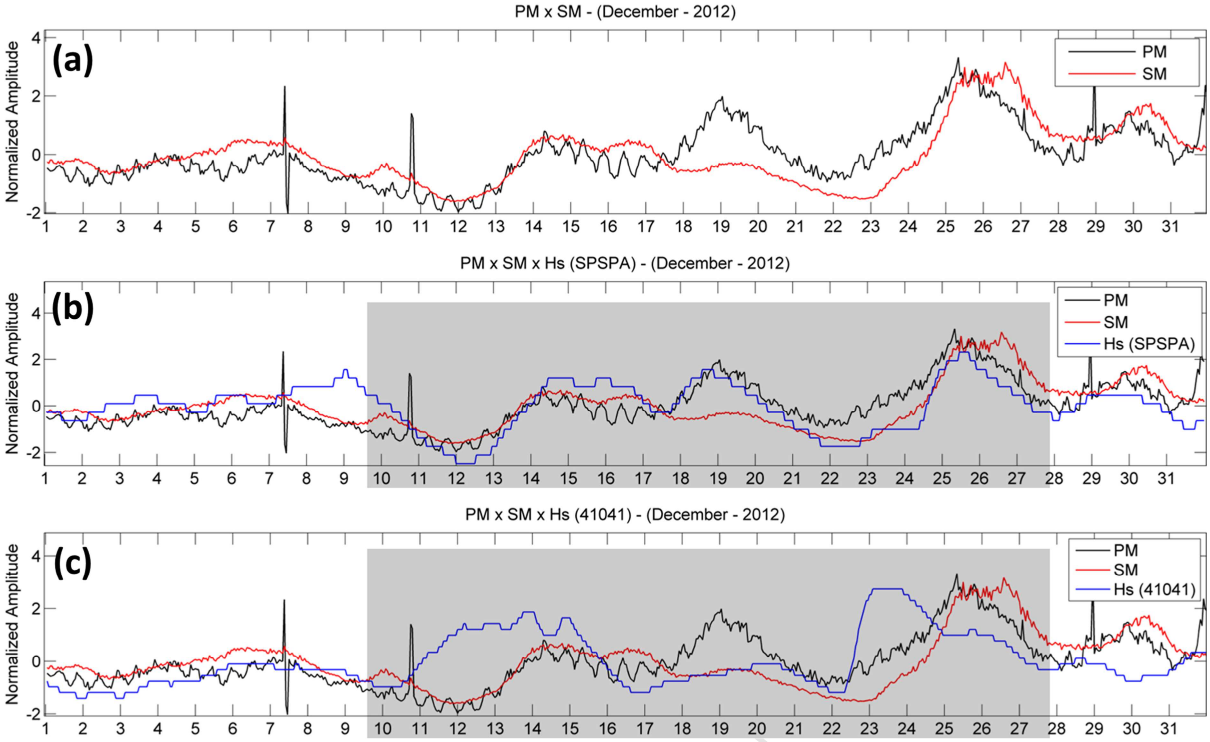
PM x SM - (December - 2012)
(a)
Normalized Amplitude
PM
SM
PM x SM x Hs (SPSPA) - (December - 2012)
(b)
PM
SM
Hs (SPSPA)
PM x SM x Hs (41041) - (December - 2012)
(c)
PM
SM
Hs (41041)

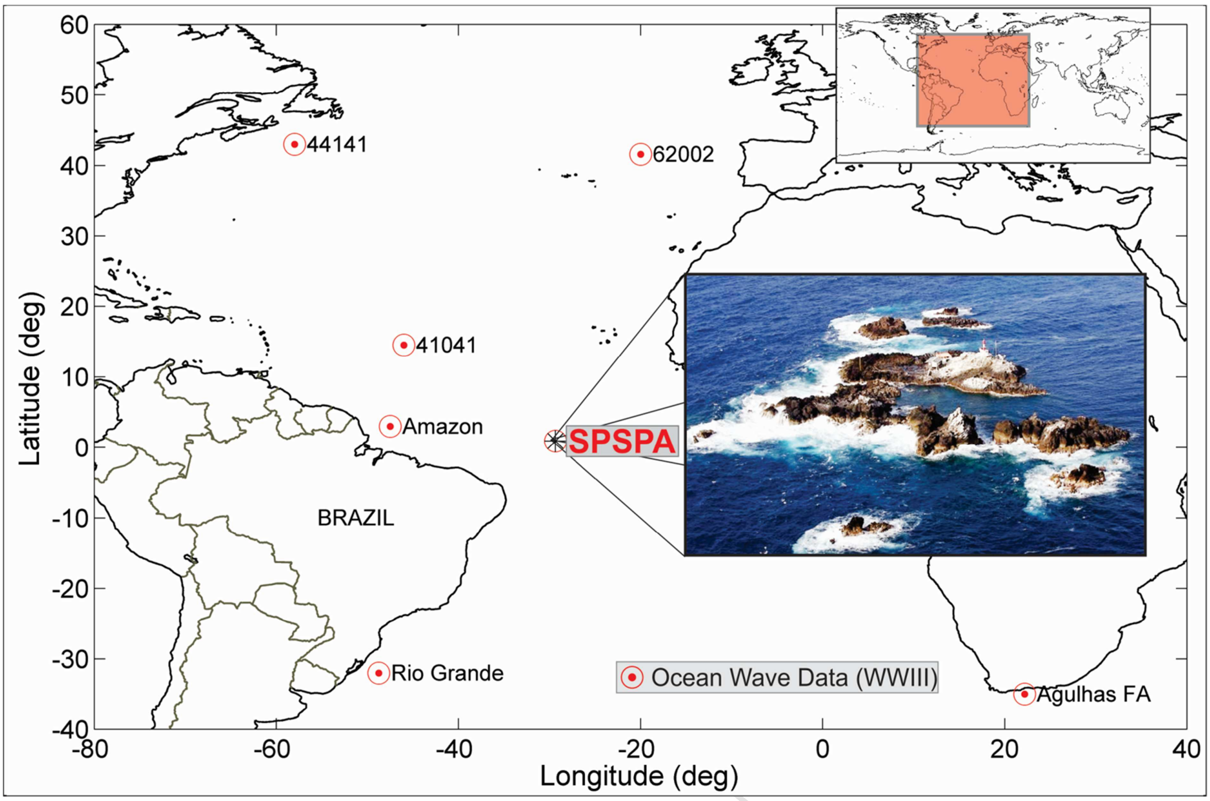

Latitude (deg)
Longitude (deg)
60
50
40
30
20
10
0
-10
-20
-30
-40
-80
-60
-40
-20
0
20
40
44141
62002
41041
Amazon
SPSPA
BRAZIL
Rio Grande
Ocean Wave Data (WWIII)
Agulhas FA

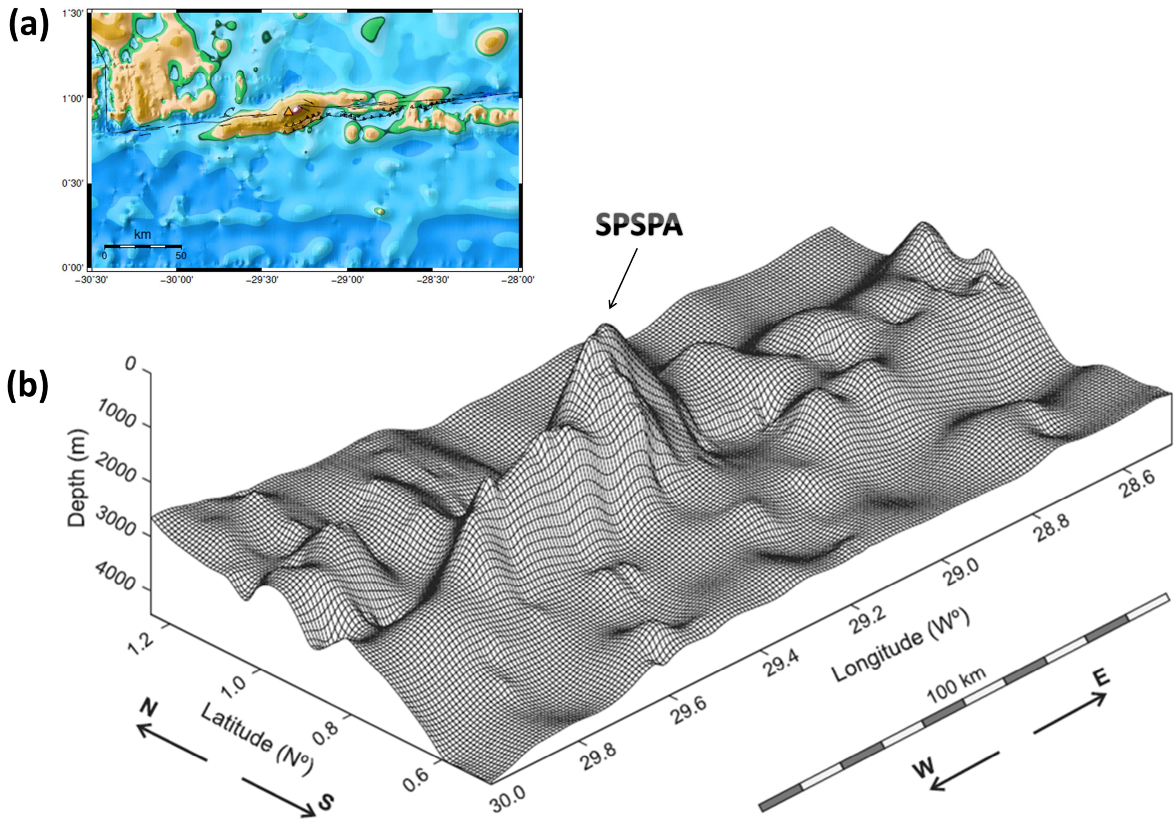
(a)
1°30'
1°00'
0°30'
0°00'
km
0
50
−30°30'
−30°00'
−29°30'
−29°00'
−28°30'
−28°00'
(b)
SPSPA
Depth (m)
0
1000
2000
3000
4000
1.2
1.0
0.8
0.6
Latitude (N°)
N
S
30.0
29.8
29.6
29.4
29.2
29.0
28.8
28.6
Longitude (W°)
100 km
W
E

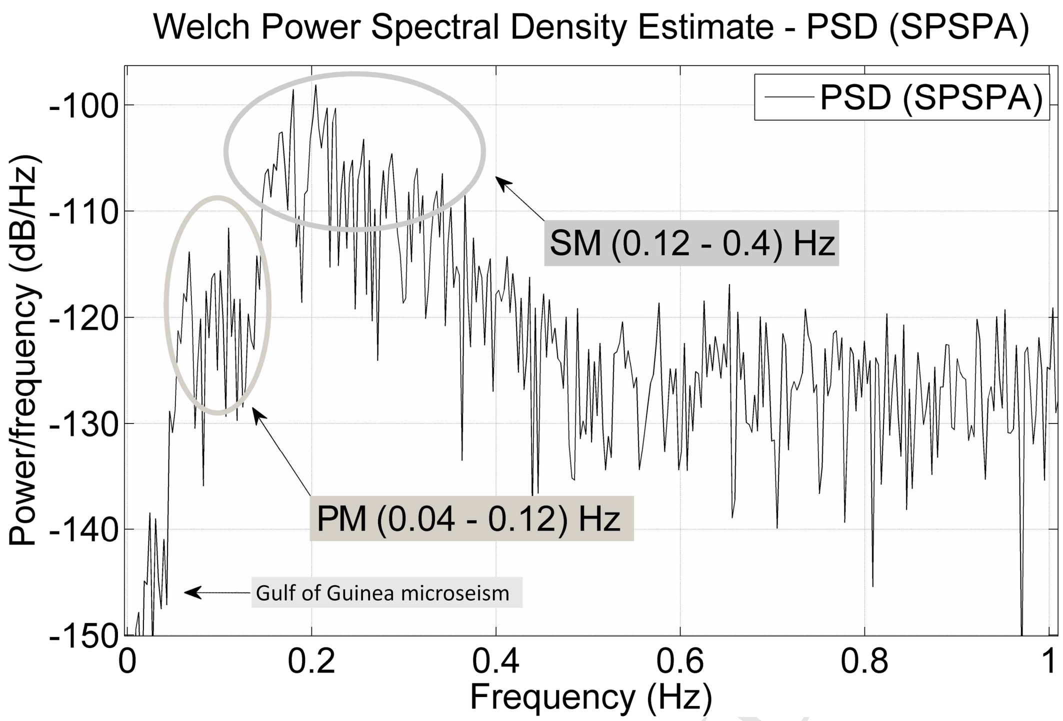

Welch Power Spectral Density Estimate - PSD (SPSPA)
PSD (SPSPA)
SM (0.12 - 0.4) Hz
PM (0.04 - 0.12) Hz
Gulf of Guinea microseism
Power/frequency (dB/Hz)
-100
-110
-120
-130
-140
-150
0
0.2
0.4
0.6
0.8
1
Frequency (Hz)

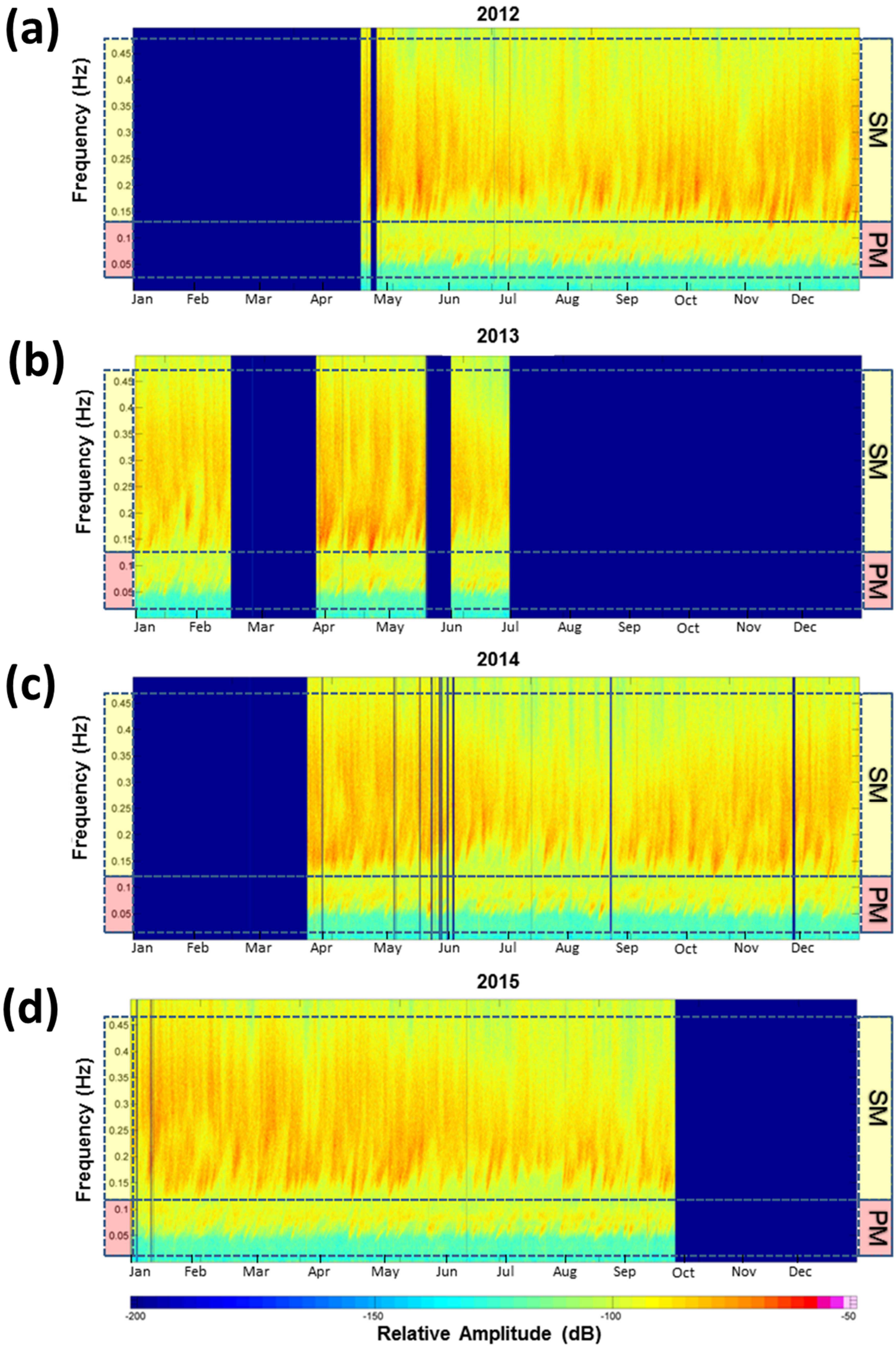
(a)
2012
Frequency (Hz)
0.45
0.4
0.35
0.3
0.25
0.2
0.15
0.1
0.05
SM
PM
Jan Feb Mar Apr May Jun Jul Aug Sep Oct Nov Dec
(b)
2013
(c)
2014
(d)
2015
-200 -150 -100 -50
Relative Amplitude (dB)

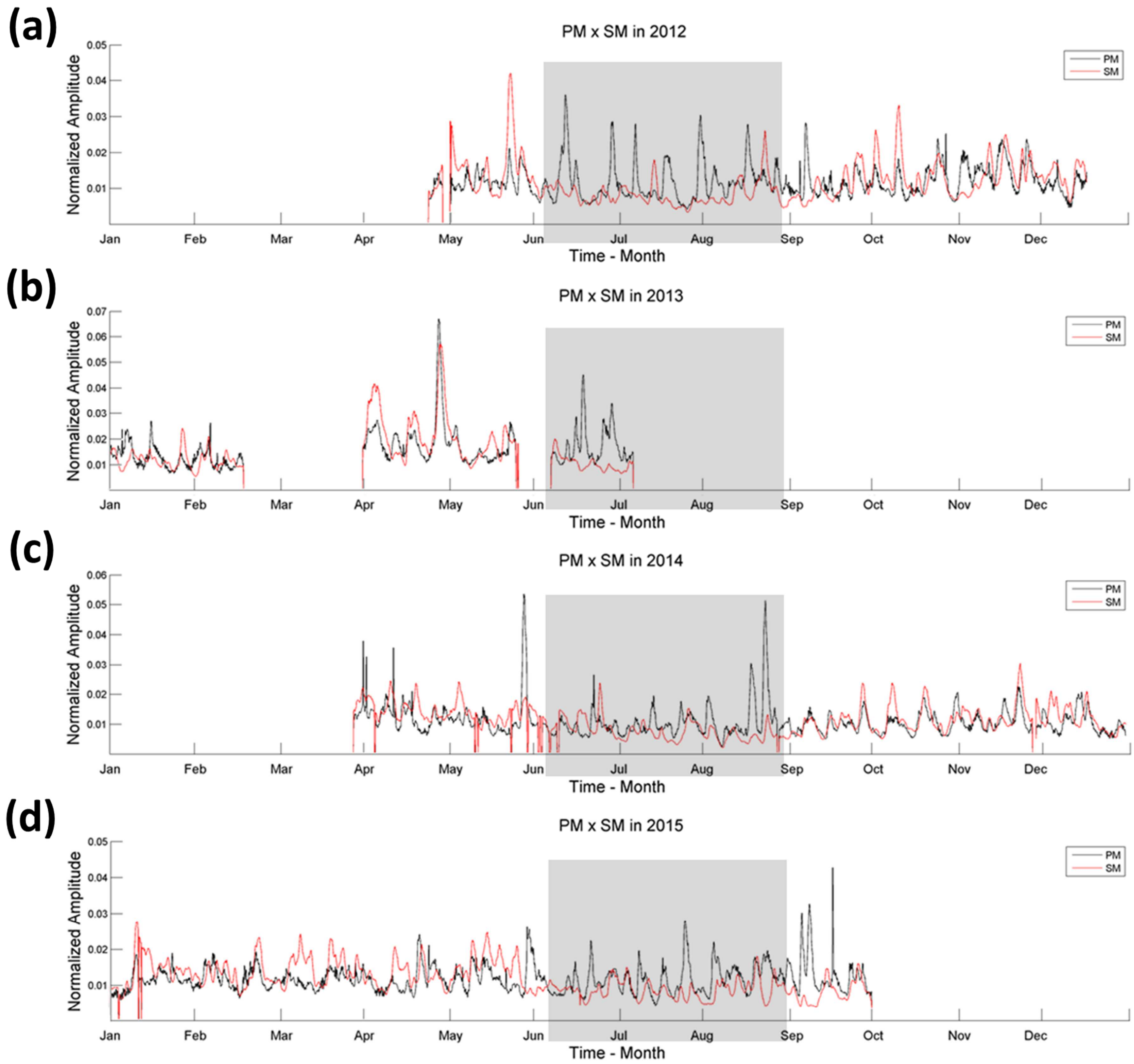
(a)
PM x SM in 2012
Normalized Amplitude
PM
SM
Jan
Feb
Mar
Apr
May
Jun
Jul
Aug
Sep
Oct
Nov
Dec
Time - Month
(b)
PM x SM in 2013
(c)
PM x SM in 2014
(d)
PM x SM in 2015

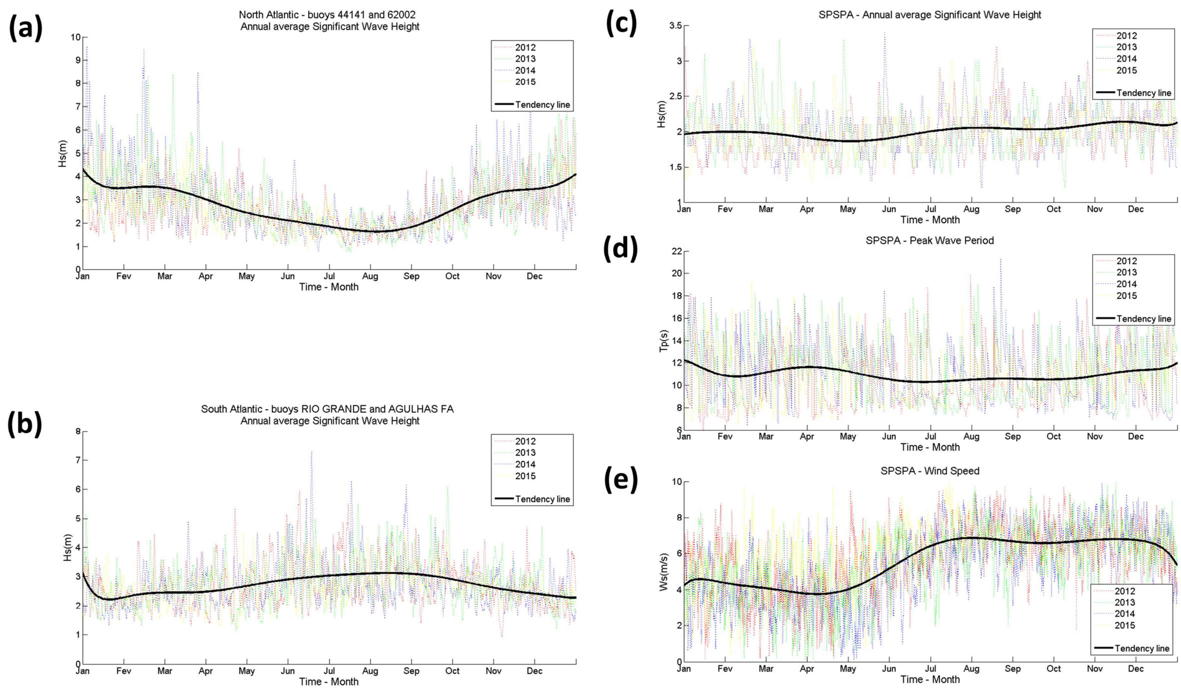
(a)
North Atlantic - buoys 44141 and 62002
Annual average Significant Wave Height
Hs(m)
Time - Month
2012
2013
2014
2015
Tendency line
(b)
South Atlantic - buoys RIO GRANDE and AGULHAS FA
Annual average Significant Wave Height
Hs(m)
Time - Month
(c)
SPSPA - Annual average Significant Wave Height
Hs(m)
Time - Month
(d)
SPSPA - Peak Wave Period
Tp(s)
Time - Month
(e)
SPSPA - Wind Speed
Ws(m/s)
Time - Month
Jan Fev Mar Apr May Jun Jul Aug Sep Oct Nov Dec

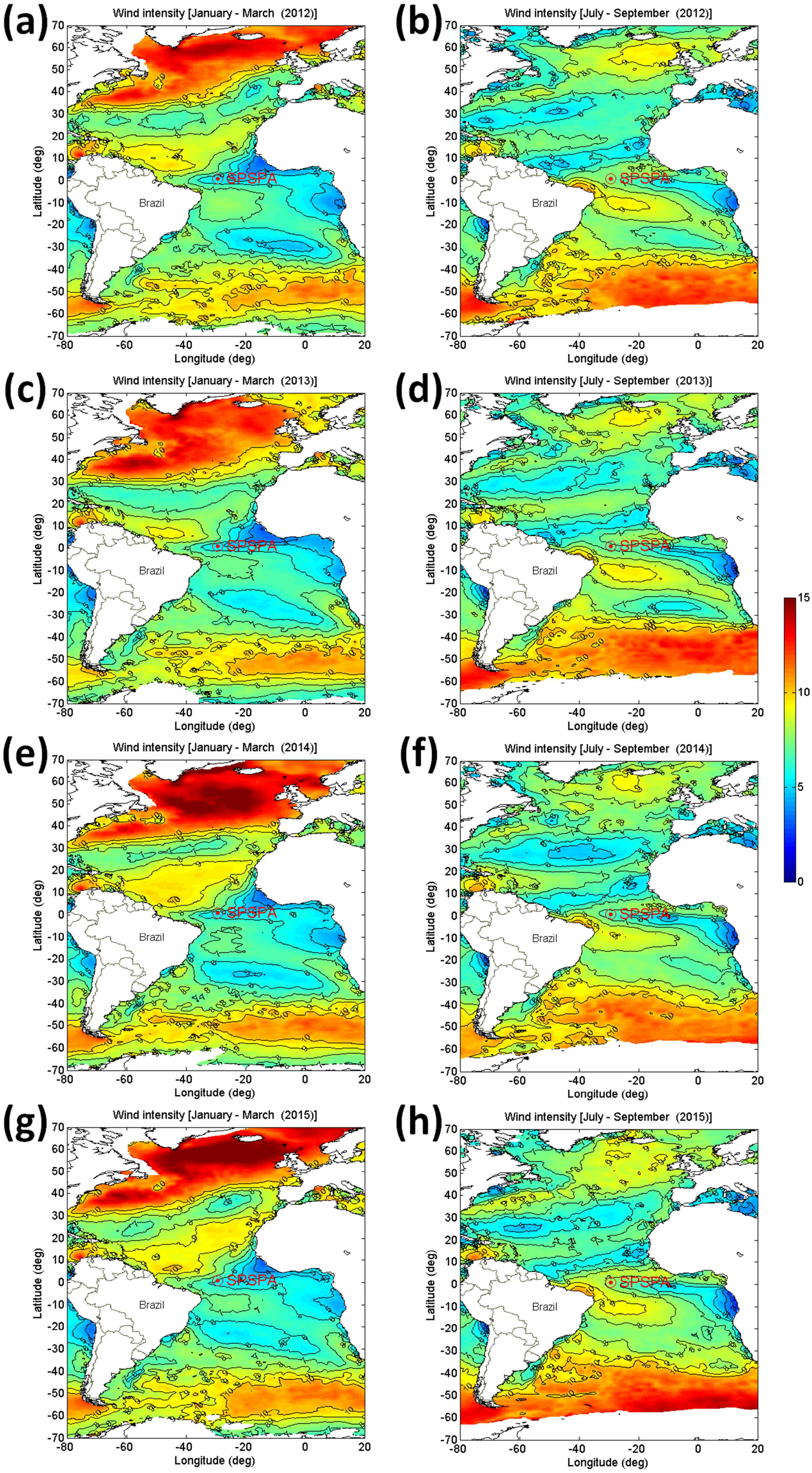
(a)
Wind intensity [January - March (2012)]
(b)
Wind intensity [July - September (2012)]
(c)
Wind intensity [January - March (2013)]
(d)
Wind intensity [July - September (2013)]
(e)
Wind intensity [January - March (2014)]
(f)
Wind intensity [July - September (2014)]
(g)
Wind intensity [January - March (2015)]
(h)
Wind intensity [July - September (2015)]
Latitude (deg)
Longitude (deg)
Brazil
SPSPA
15
10
5
0

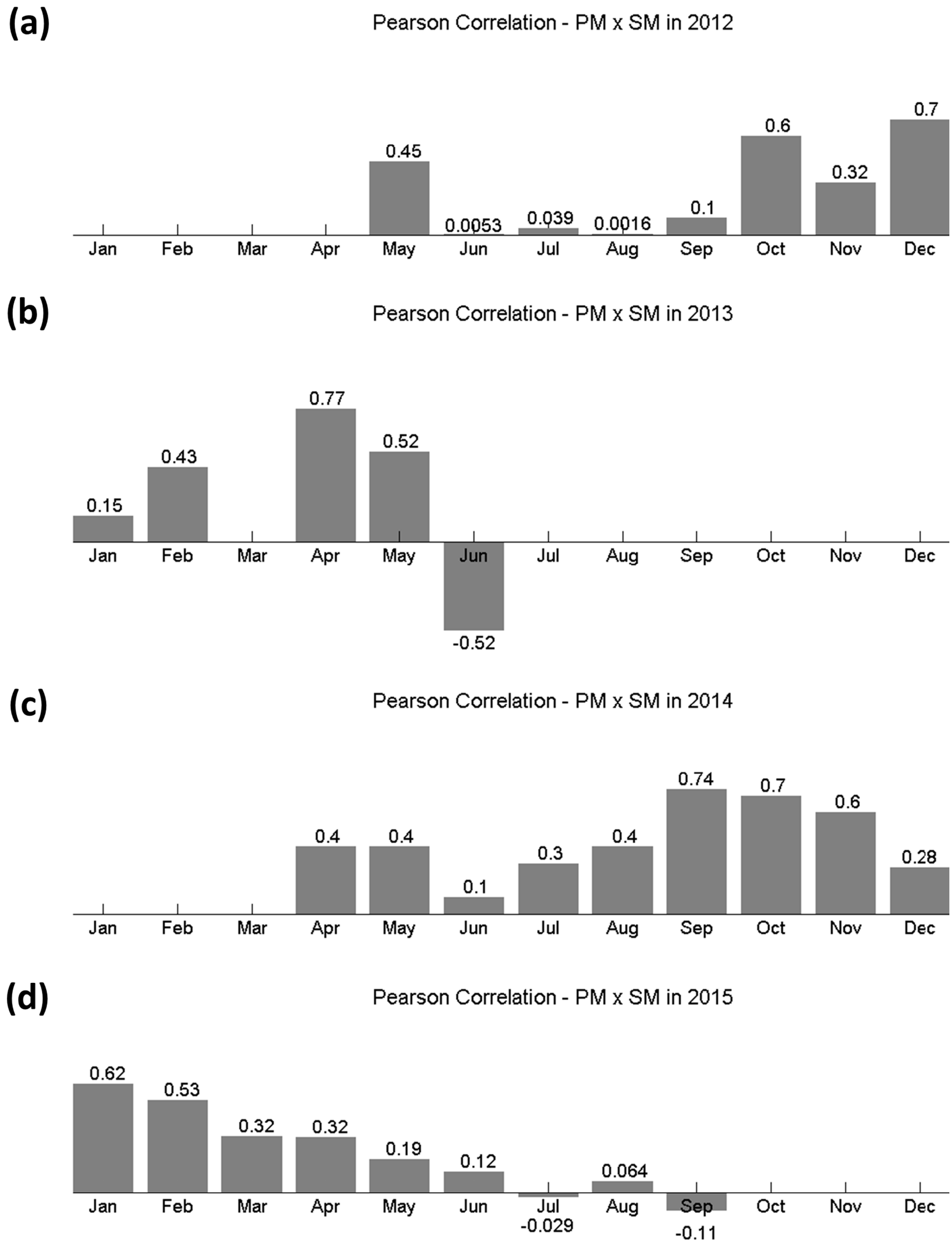
(a)
Pearson Correlation - PM x SM in 2012
0.45
0.0053
0.039
0.0016
0.1
0.6
0.32
0.7
Jan Feb Mar Apr May Jun Jul Aug Sep Oct Nov Dec
(b)
Pearson Correlation - PM x SM in 2013
0.15
0.43
0.77
0.52
-0.52
Jan Feb Mar Apr May Jun Jul Aug Sep Oct Nov Dec
(c)
Pearson Correlation - PM x SM in 2014
0.4
0.4
0.1
0.3
0.4
0.74
0.7
0.6
0.28
Jan Feb Mar Apr May Jun Jul Aug Sep Oct Nov Dec
(d)
Pearson Correlation - PM x SM in 2015
0.62
0.53
0.32
0.32
0.19
0.12
-0.029
0.064
-0.11
Jan Feb Mar Apr May Jun Jul Aug Sep Oct Nov Dec

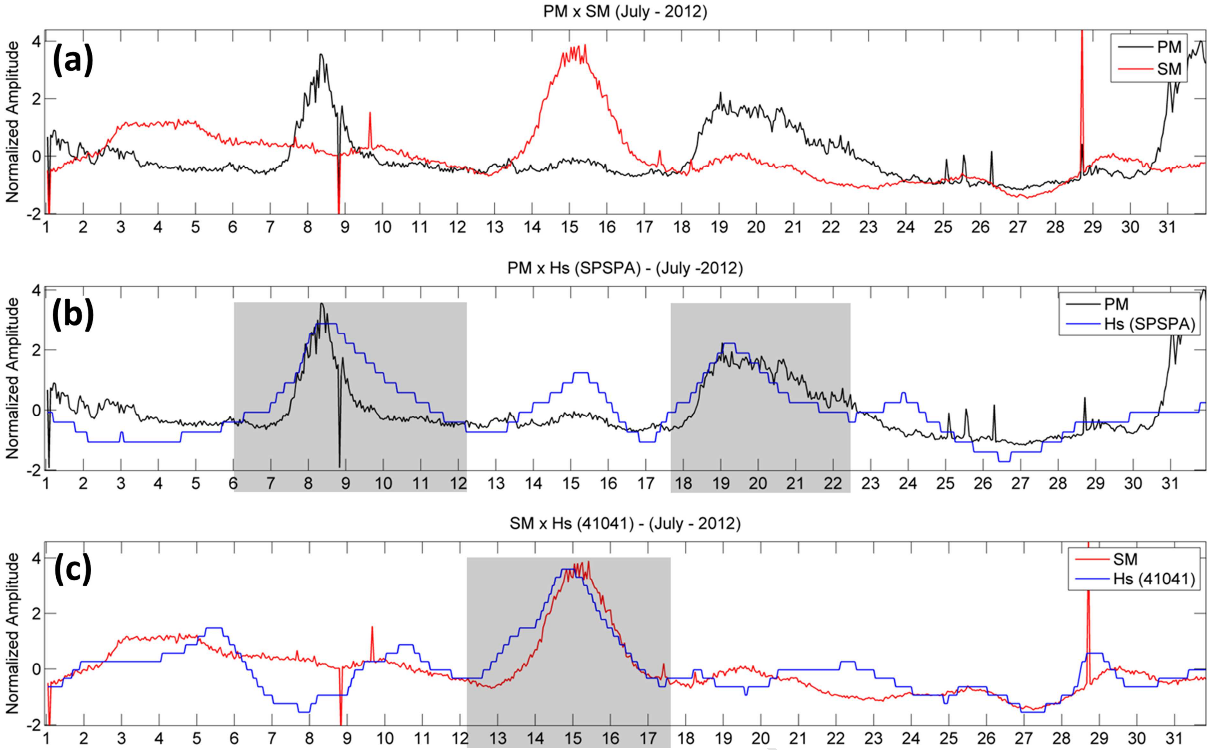
PM x SM (July - 2012)
(a)
Normalized Amplitude
PM
SM
PM x Hs (SPSPA) - (July -2012)
(b)
PM
Hs (SPSPA)
SM x Hs (41041) - (July - 2012)
(c)
SM
Hs (41041)

Highlight of the m/s “Microseismic noise in the Saint Peter and Saint Paul Archipelago, Equatorial Atlantic” by D. E. Queiroz et al.

- This is the first study carried out which characterizes the noise at station SPSPA, permitting future climate monitoring studies, unbiased from anthropogenic activities;
- This study showed seasonality between microseismic noise, wind speed and wave height in a particular region located in the center of the Atlantic Ocean close to the Equator;
- The SPSPA noise recordings indicate that the microseismic noise on the island is dominated by Northern Hemisphere climate.